Materials Science and Engineering B108 (2004) 124–129

www.elsevier.com/locate/mseb

Hydrogen adsorption in carbon nanostructures compared

H.G. Schimmel [a,*], G. Nijkamp [b], G.J. Kearley [a], A. Rivera [a], K.P. de Jong [b], F.M. Mulder [a]

[a] *Interfaculty Reactor Institute, Delft University of Technology, Mekelweg 15, 2629 JB Delft, The Netherlands*
[b] *Inorganic Chemistry and Catalysis, Debye Institute, Utrecht University, P.O. Box 80083, 3508 TB Utrecht, The Netherlands*

Abstract

Recent reports continue to suggest high hydrogen storage capacities for some carbon nanostructures due to a stronger interaction between hydrogen and carbon. Here the interaction of hydrogen with activated charcoal, carbon nanofibers, single walled carbon nanotubes (SWNT), and electron beam 'opened' SWNT are compared and shown to be similar. The storage capacity below 77 K of these materials correlates with the surface area of the material with the activated charcoal having the largest. SWNT and 'opened' SWNT have a relatively low accessible surface area due to bundling of the tubes. Pressure–temperature curves give the interaction potential, which was found to be ≈ 580 K or 50 meV in all samples, leading to significant adsorption below ≈ 50 K. Using the inelastic neutron scattering signal associated with rotation of the hydrogen molecule as a sensitive probe for the surroundings of the molecule, no difference was found between the hydrogen molecules adsorbed in the investigated materials. These combined spectroscopic and macroscopic results show that SWNT, nanofibers and activated carbons store molecular hydrogen due to their graphitic nature and not because they possess special morphologies. Results from a density functional theory computer calculation suggest molecular hydrogen bonding to an aromatic C–C bond of graphite, irrespective of the surface morphology farther away.

Keywords: Hydrogen adsorption; Single walled nanotubes; Physisorption; Carbon; Density functional calculations

1. Introduction

Hydrogen, often quoted as the fuel of the future, produces only water as a byproduct when used in a fuel cell. In view of discussions about greenhouse gases and pollution caused by consumption of fossil fuels, hydrogen is indeed an ideal energy carrier. Apart from questions regarding the environmentally friendly production of hydrogen, the application of this fuel is hampered by storage problems. Hydrogen being very volatile is hard to store. High pressures (700 bar) or low temperatures (20 K) are needed to store a reasonable amount, but are either impractical/unsafe or not cost effective. This transportation and storage problem has stimulated research world wide. A material is sought in which hydrogen is stored in reasonable amounts at or close to ambient conditions. In the past focus has been on metallic hydride alloys such as $LaNi_5$, FeTi, and MgNi. Since 1997 hydrogen storage capacities as high as 5–60 wt.% at room temperature in carbon nanostructures have been reported. However by now it is clear that carbon nanostructures only store hydrogen at low temperatures or high pressures [1–4]. In this paper we compare both opened and as prepared single walled carbon nanotubes (SWNT) with other forms of nanostructured carbon. We use pressure–temperature techniques as a macroscopic tool and neutron scattering to measure the state and the environment of adsorbed hydrogen molecules. The intercalation of potassium in graphitic nanofibers is known to increase the hydrogen storage up to a factor of 10 (when H_2 is counted per unit C) [5]. We present calculations on the interaction of hydrogen with carbon surfaces and on hydrogen in graphite intercalated with potassium.

2. Methods

The pressure of a gas in equilibrium with adsorbed gas molecules as a function of temperature T is given by de Boer [6] as:

$$P = Cf\sqrt{T}\,\mathrm{e}^{-H_{\mathrm{ad}}/kT}\frac{\theta}{1-\theta}, \tag{1}$$

with C being a constant and H_ad the adsorption potential. When the volume for the gas phase around the sample with

* Corresponding author. Tel.: +31-15-2783809; fax: +31-15-2788303.
E-mail address: h.g.schimmel@iri.tudelft.nl (H.G. Schimmel).

0921-5107/$ – see front matter © 2003 Elsevier B.V. All rights reserved.
doi:10.1016/j.mseb.2003.10.091

adsorbed hydrogen is small, we can assume the fractional coverage θ to be constant in the temperature range investigated. From the decrease of the pressure as the temperature of the sample decreases the value of H_{ad} can be estimated using a least squares fitting routine.

Diatomic molecules such as hydrogen can rotate around two axes. The energy associated with this rotation is quantized and labelled by the rotational number J. For the free molecule the energy E_J of the J-th level takes in good approximation the value $E_J = J(J+1)B$. The rotational spectrum of an adsorbed molecule will be distorted by influences from the environment. This is because electromagnetic fields can cause a shift of a rotational level. Furthermore such fields can lift degeneracies of levels, thereby splitting a level. In general a stronger interaction between adsorbed molecule and adsorbent leads to a more distorted spectrum. We make use of this rotational spectrum obtained from inelastic neutron scattering as a measure for: a) the presence of molecular H_2 instead of atomic H, and b) the interaction between hydrogen and its environment because it is both a sensitive and a local probe.

Light can only stimulate odd to odd and even to even transitions of diatomic molecules due to the selection rules. Neutrons, on the other hand, are able to induce every rotational transition. In addition neutrons have a large penetrating power in most materials. Therefore, it is possible to study adsorbed hydrogen at low temperatures easily. This lead us to the use of inelastic neutron scattering as a tool to investigate hydrogen in different forms of carbon stored at low temperatures. Using the so-called RKS, a rotating crystal spectrometer located at the HO-reactor in Delft, The Netherlands, we have taken spectra of the energy of neutrons scattered by the sample.

Calculations have been performed on the systems described in this article by means of density functional theory computer code as implemented in Dmol[3].

3. Sample materials

Five different materials have been investigated in this study: two activated carbons: AC Norit 990293 (NAC) and AC Norit GSX (GSX), a ‘fishbone’ carbon nano-fibre sample (GNF) and two samples consisting of single walled carbon nanotubes, electron beam opened and as bought. Activated carbons are highly micro- and mesoporous carbon materials. They have been prepared from raw materials (e.g. peat, lignite, coal) and carbonized and reacted with steam at 1000 °C. In this way some of the carbon atoms are removed from the natural templated material by gasification, which yields a very porous structure.

Graphitic nanofibers were grown using a fixed bed reactor. Nickel particles on a silica support (Aerosil 200) dissociate methane, forming hydrogen and carbon atoms that dissolve in the nickel particle. These carbon atoms diffuse through the nickel catalyst particle to form a carbon nanofiber. The silica support was removed in a refluxed boiling KOH solution. In the same manner a treatment with HNO_3 was used to remove the Ni particles [7]. The nanofibers used in this investigation had a fishbone arrangement of the graphite planes with respect to the fiber axis. The diameter of these fibers ranges between 20 and 30 nm, with an average of 25 nm. These fibers were loaded with 0.2 wt.% Pd nanoparticles using ion-exchange from a $Pd(NH_3)_4Cl_2$ solution [8]. This was done in order to open up the possibility to have atomic H in the sample, that may possibly even intercalate in between the graphite layers as has been speculated by others [9–11].

The single walled carbon nanotubes were obtained commercially[1]. The nanotubes were produced by the HiPCo process in which $Fe(CO)_5$ decomposes in a CO atmosphere [12]. Our sample contains 17.5 wt.% or less than 5 at.% of leftover iron catalyst particles. The sample was characterized by X-ray diffraction, which showed no sharp peaks, indicating that no crystalline form of graphite or iron in a detectable amount was present. Mössbauer spectroscopy revealed that the left-over catalyst particles are exclusively present in the form of Fe_3C. Transmission electron microscopy was used to investigate the diameter of the nanotubes and the iron carbide particles. The carbon nanotubes are packed with a smallest repetition distance of about 1.25 nm, indicating that the size of the tubes is around 1.25 nm. The iron carbide particles are larger, with diameters around 4 nm. The surface area of the relatively low number of massive iron carbide particles is much smaller than that of the nanotubes, and any adsorption of H_2 on these particles can therefore not be observed.

A small amount, 0.8 g, of the single walled nanotubes were treated with an intense beam of electrons from the 1.4 MeV Van der Graaff accelerator. During irradiation a continuous flow of argon gas was present in the airtight cell with thin kapton windows, in order to avoid oxidation of the defects. Prior to irradiation the sample was evacuated at elevated temperatures to remove unwanted adsorbed molecules. The sample was irradiated with a dose of $10^{21}/cm^2$ of electrons, an amount which has been reported to induce V4-type vacancies in graphite [13]. This means that there are vacancies of the size of four atoms in the nanotube walls. It was expected that hydrogen is able to enter the nanotubes through such vacancies because the size of such vacancies is larger than the size of a hydrogen molecule (which is commonly taken as 0.29 nm).

4. Experiments

4.1. Adsorption measurements

Samples were loaded in aluminum containers and mounted in a closed cycle refrigerator. The samples were

[1] from Carbon Nanotechnologies Incorporated, Houston, USA.

evacuated to below 1 mPa while heated to 323 K for at least 12 h. Adsorption isotherms were recorded by opening a valve to a known volume of hydrogen gas with a known pressure, waiting for equilibrium and measuring the pressure, and repeating this procedure up to 1 bar. Temperature–pressure curves were measured inside the same system.

4.2. Inelastic neutron scattering

The samples under investigation were loaded in aluminum sample chambers, mounted into a cryogenic system and evacuated to below 1 mPa while heated to 323 K for at least 12 h. The sample thickness was such that up to 10% of the neutrons was scattered by the nuclei of the sample when hydrogen was loaded. The samples were cooled down to 3.6 K and a background measurement was performed on the evacuated sample. Then the sample was heated to 77 K and hydrogen was loaded up to a pressure of 1 bar. This temperature and pressure was chosen because it are the reference conditions in our previous work. When insufficient hydrogen had been adsorbed for a good neutron spectrum, filling was continued at 1 bar at a temperature that was lowered by a few degrees (this enhances the adsorption capacity considerably). In this manner 100–200 ml STP H_2 was adsorbed in the sample, sufficient for recording an accurate neutron spectrum in a reasonable time. The hydrogen loaded sample was then cooled down to 3.6 K and a spectrum was recorded. We can exclude the possibility of having measured on solid hydrogen because the hydrogen vapor pressure above the sample is always much lower than the equilibrium vapor pressure for liquid or solid hydrogen.

The measurements were performed on the time-of-flight spectrometer RKS at the 2 MW nuclear reactor in Delft, The Netherlands. This spectrometer uses two choppers and a rotating pyrolitic graphite monochromator to produce a pulsed, mono-energetic beam. The incident energy of the neutron beam was selected to be 157.3 cm^{-1}. The scattered neutrons are detected by an array of detectors giving a momentum transfer range of 0.2–3.5 $Å^{-1}$ and their arrival time is recorded. The time-of-flight of the neutrons were transformed into energies and the structure factor $S(Q, \omega)$ was obtained by multiplying with k_i/k_f and by normalizing on the incident beam monitor. In order to improve statistics the spectra were summed over the momentum transfer Q so that the average value of the spectra is 1.6 Å. Scattering of the sample without hydrogen was subtracted from the spectrum of the hydrogen-loaded sample. In this way only the scattering of hydrogen is visible in the corrected spectra. All experiments were performed at a temperature of 3.6 K. These low temperatures are needed to avoid unwanted broadening of the spectra.

4.3. Theoretical calculations

In order to understand the experimental results we performed computer calculations by means of density functional theory, using Dmol[3]. We used the numerical basis set DND (double numerical with d functions) and the Perdew Wang local correlation density functional.

5. Results and discussion

5.1. Pressure and temperature dependent hydrogen adsorption

All of these samples were tested for hydrogen storage capacity at 77 K and 1 bar. For the SWNTs this was the first time we determined this, while for the other compounds the adsorbed amounts (obtained volumetrically) under these conditions were the same as we found previously [14]. The sample of electron irradiated nanotubes and the nanotubes as-received showed the same amount of hydrogen storage at 77 K (60 ml/g). The fact that the hydrogen storage capacity is equal for both irradiated and as-received carbon nanotubes, indicates that our electron irradiation treatment did not increase the accessible surface area in the sample. We assume the two samples to be equivalent and in what follows only measurements on as-received SWNT are presented.

For two samples (SWNT and NAC) we recorded the pressure as a function of the sample temperature during cooling. The pressure of hydrogen gas above Norit GSX during warming was also measured. These measurements are presented in Fig. 1. The least squares fit on the GSX data with the model of Eq. (1) derived above is shown in the figure. Results from these fits are given in Tables 1. From the errors associated with the fitted values of the adsorption potentials, we conclude that the adsorption potential is 580±60 K or 5±0.5 kJ mol^{-1}. The review article of Vidali et al. on potentials of physical adsorption gives a well depth of 51.7 meV for pure bulk graphite, which equals 600 K or 5 kJ mol^{-1} [15], in agreement with our results. Clearly the value of Dillon et al. of 19.6 kJ mol^{-1} for hydrogen adsorbed onto single walled carbon nanotubes is not reproduced [16].

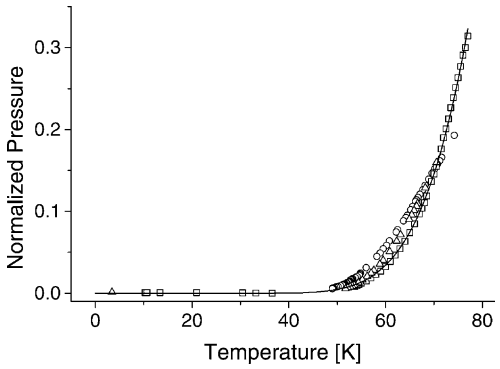

Fig. 1. Temperature–pressure curves for SWNT (circles), Norit AC 990293 (triangles) and Norit GSX (squares). The line is a fit with the model $P = C'\sqrt{T}\,e^{-H_{ad}/kT}$ through the measured curve for Norit GSX. Using this model the adsorption energies were obtained (580±60 K).

Table 1
Properties of the investigated materials

	NAC	GSX	SWNT	GNF
V (ml STP)	238	160	60	20
S_{BET} (m^2/g)	2200	933	380	196
H_{ad} (K)	513	576	525	–
p (cm^{-1})	119	120	119	117

V is the volume at standard temperature and pressure (1 bar and 295 K) of hydrogen stored in 1 g of material at 77 k and 1 bar, S_{BET} is the BET surface area (the value for SWNT is from [21]), H_{ad} is the enthalpy of adsorption derived from pressure–temperature curves and p is the peak position in the neutron spectra due to the rotational transition. The properties of the irradiated SWNTs are the same as those for SWNTs.

The relatively low hydrogen storage capacity of SWNT, shows that only the outer surface of the bundles of tubes are accessible for hydrogen molecules. The defects caused by the intense high energy electron radiation apparently have not increased the accessible surface area. We have to assume that the hole in the tube walls are closed effectively by spontaneous rearrangement of the carbon atoms immediately after the holes were formed. Such effects were observed using TEM images and damage created by the TEM beam itself [13].

5.2. Inelastic neutron scattering results

Fig. 2 shows the measured spectra for the four different carbon materials. Table 1 lists the results from least squares fits of the peaks with a Gaussian peak profile. The Gaussian peak profile was chosen because it is a good description of the resolution function of the instrument at these energy transfers (determined form a measurement on solid H_2. The determination of the absolute position of the peaks is influenced by systematic errors due to uncertainties in the neutron incident energy and path-lengths in the instrument. We estimate this error to be 2%, which is 2 cm^{-1}, of the neutron energy loss. The fitted peak positions show that a shift of the rotational transition energy cannot be observed within experimental accuracy. The peak widths are comparable with the experimental resolution, which was determined to be 11 cm^{-1} (full width at half maximum) from a gauge measurement on solid hydrogen. No splitting of the $J = 1$ level within the experimental resolution due to hindering of the rotation was observed.

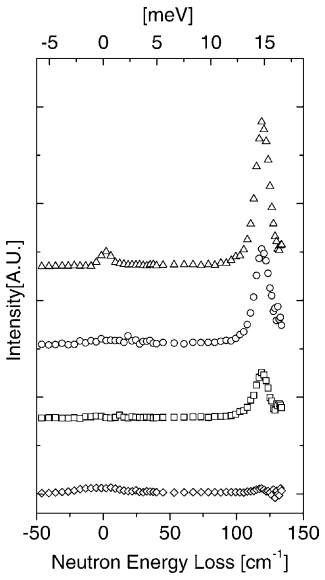

Fig. 2. Neutron energy loss spectra of hydrogen adsorbed in Norit AC990293 (triangles), single walled carbon nanotubes (circles), Norit GSX (squares) and graphitic nanofibers(diamonds). The data are normalized on the incident number of neutrons on the sample. The (mostly elastic) scattering of the sample without hydrogen has been subtracted (see text) which makes that only the scattering by hydrogen is visible. The graphitic nanofibers adsorb even after extra filling a very small amount of hydrogen, resulting in a very weak peak.

The intensities in the elastic peak (zero energy transfer) are much lower than the rotational transition peak. This excludes the presence of molecular ortho-hydrogen and of atomic hydrogen in significant amounts, because scattering cross-sections for both are much larger than for the transition of $J = 0$–1. Furthermore, the elastic peak intensity compared to the inelastic peak intensity is as should be expected for the scattering by the para-hydrogen in the samples. Also when observing the spectra of the samples as a function of time (obtained from the different subruns for each spectrum) it was clear that the conversion of ortho- to para-hydrogen was completed during the few hours of cooling. This is caused by the enhanced nuclear spin relaxation induced by the paramagnetic catalyst residuals (SWNT, GNF) or impurities (NAC, GSX).

The $J = 1$ rotational peak is in the same position in carbon materials that have completely different topologies: the highly regular curved sheets of carbon in SWNTs, conical curved carbon sheets in fishbone nano-fibres, and highly porous activated carbons. Evidently the morphology of the carbon surfaces has little effect on the rotation potentials for hydrogen and the binding will be small as inferred from the adsorption measurements. This would also indicate that the bonds responsible for the adsorption are similar in the different materials, in agreement with the macroscopic adsorption data. The claims for extremely large adsorption capacities in SWNTs can now be discarded both on the basis of macroscopic adsorption data and microscopic interaction strength's.

To check these assumptions, detailed calculation have been performed using Density Functional Theory. First we optimized the position of a hydrogen molecule above a small piece of graphite built from four carbon hexagons (Fig. 3). The position with lowest energy for the hydrogen molecule was 2.91 Å above a central C–C bond. Then we turned the hydrogen molecule stepwise by 180° and evaluated the potential energy each 20°. In this way we obtained an estimate of the barrier for rotation for the adsorbed molecule. The barrier we find is indeed very small and is, within computational accuracy, consistent with the experiments.

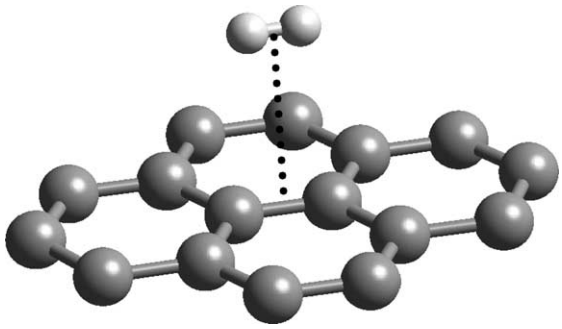

Fig. 3. The graphite surface and the hydrogen molecule in their minimum energy position. The hydrogen molecule is located right above the center of the C–C bond. From this configuration the energy was calculated using DFT when the hydrogen molecule was turned around.

Graphitic nanofibers intercalated with potassium to a composition of C_8K, show a tenfold increase in hydrogen storage capacity with respect to the original amount of carbon [5]. The stoichiometry of the intercalated parts is not known, but is thought to contain less K than C_8K. Excess potassium may be present in other forms outside the fibers. While experiments are being performed on this material, we performed calculations using Dmol[3] on the system to investigate the adsorption potentials.

5.3. Calculations on potassium intercalated nanofibers

We employed flat graphite planes at a distance of 5.1 Å to calculate the total energy of the system as a function of the position of the hydrogen molecule (see Fig. 4). Such a structure reproduces well the samples we are using for our experiments consisting of Graphitic Nanofibers with a fishbone structure intercalated with potassium. After intercalation the fibers keep their shape, but the distance between adjacent graphite layers in the fishbone structure becomes larger than 3.4 Å.

Initially the hydrogen molecule was positioned in such a way that the distance between the K atom and its nearest H atom was 1.5 Å. Subsequently, the hydrogen molecule was moved in the direction parallel to the graphite planes away from the potassium atom. The total energy of the system was calculated for every position of the molecule. We define as

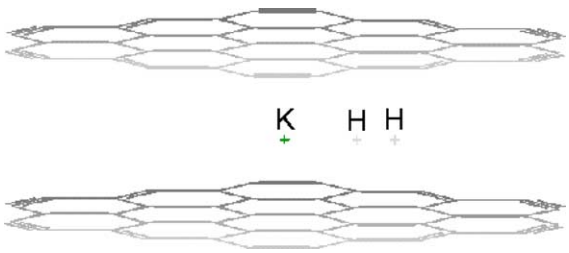

Fig. 4. Two graphite planes at 5.1 Å from each other. A K atom was placed in the center and a hydrogen molecule parallel to the planes at different distances from the potassium atom. The total energy of the system was calculated for every position of the hydrogen molecule.

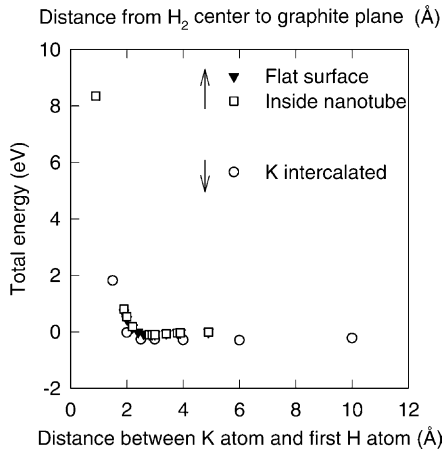

Fig. 5. Total energy of the following systems: (i) a hydrogen molecule on a flat graphite surface, (ii) a hydrogen molecule inside a nanotube, represented by a curved graphite surface with 6.5 Å radius and (iii) a hydrogen molecule and a K atom between two graphite planes separated at 5.1 Å of each other. The total energy is plotted as a function of the distance between the H_2 center and the graphite surface for cases (i) and (ii), top axis and as a function of the distance between the first H atom and the K atom for case (iii), bottom axis.

zero point energy the total energy of the system when the K atom and the hydrogen molecule are each about 10 Å apart from the carbon structure. Fig. 5 shows the total energy of the system with respect to the zero point energy. For comparison the total energy of systems containing a hydrogen molecule on a graphite surface are presented. Two graphite surfaces were chosen in this case: a flat graphite surface and a curved surface (radius 6.5 Å, so comparable to a SWNT radius). A hydrogen molecule was moved perpendicularly to the corresponding graphite surface and the total energy of the system was calculated for every position of the hydrogen molecule. The zero point energy was taken in this case when the center of the hydrogen molecule was at a distance larger than 5 Å from the corresponding graphite surface.

The calculations shown in Fig. 5 indicate the existence of an energy well in every case. The system graphite plane-hydrogen molecule has an energy minimum when the center of the hydrogen molecule is at 2.9 Å from the graphite surface. This corresponds to an energy well of 0.08 eV, or ≈900 K. In the case of a curved graphite surface, the system also reaches an energy minimum when the hydrogen molecule is at 2.9 Å. However, in this case the potential well is deeper, it reaches 0.10 eV (≈1200 K). This is not surprising, and is due to the higher concentration of neighboring C atoms around the hydrogen molecule. The calculations predict the existence of an energy minimum in the case of K intercalated in graphite planes when the first hydrogen atom is 6 Å from the K atom. Interestingly, the energy well corresponding to this case is the deepest amounting 0.30 eV (similar to ≈3500 K). These calculations emphasize that for hydrogen storage purposes intercalation of foreign atoms could yield interesting results. In particular, the presence of K atoms results in an increased

interplanar distance (larger than 5 Å). This facilitates the incorporation of hydrogen to the internal graphite surfaces, which is otherwise impossible. In addition, the indication of an energy well much deeper than that existing at the surface of graphite structures is supposed to be beneficial for the binding of hydrogen at higher temperatures than in the case of non-doped graphite nanostructures.

5.3.1. Molecular Dynamics simulations

Apart from the elaborate DFT calculations we also performed fast molecular dynamics (MD) simulations in order to observe the motion of the H_2 molecule along a surface of a SWNT bundle. The MD was performed within the Cerius2 suite using the COMPASS force field [17]. This force field was recently successfully applied on the MD of other highly aromatic compounds [18]. It appeared that at temperatures lower than 40 K the H_2 molecule diffuses along the bundle surface with increasing kinetic energy for increasing T's, while above 40 K the chance for leaving the surface into a gas phase becomes large. These temperatures compare well with the increasing gas pressure in the macroscopic adsorption measurements.

6. Discussion

The finding that the SWNT do not store more H_2 than activated carbons is surprising when comparing the surface area's in $m^2\ g^{-1}$ of individual SWNT and the other carbons. However, it is known that during production of the SWNT they already aggregate into bundles. Our XRD results show for this reason a repetition length of SWNT diameters. Furthermore, the average bundle diameter could be deduced from small angle neutron scattering results using the SESANS instrument [19,20] to be 80 ± 25 Å. It is apparently the outer surface of these bundles that is accessible for H_2 only. Using our SWNT diameter we calculate an inter SWNT void with a diameter of 2.1 Å, which is indeed smaller than the 2.9 Å required by the H_2 molecule. A second reason why the electron beam damaged tubes do not store more H_2 can now be deduced. Most damage will be far from the surface of the bundles and will not make a difference therefore.

In order to make the accessible surface of the SWNT larger one could either split the bundles into smaller diameter ones, or make larger diameter SWNT (2.9/2.1 times larger at least) to make the inter SWNT voids larger and therefore accessible. This large diameter SWNT will not be stable however, and may collapse onto itself, so that is not a feasible route.

7. Conclusion

We conclude that different forms of carbon are essentially the same for hydrogen molecules as long as they possess the characteristic aromatic carbon rings. Thus the amount of hydrogen storage is governed by the number of accessible aromatic C–C bonds in the sample, which is related to the surface area. The morphology of the adsorption sites on more than one C–C bond distance has less importance.

Acknowledgements

We thank Mr. M. Hom and Mr. C.F. de Vroege for their assistance during electron irradiation and neutron scattering experiments. We thank Dr. S.W.H. Eijt for useful discussions. We acknowledge financial support from the Delft Institute of Sustainable Energy.

References

[1] R. Stroebel, L. Joerissen, T. Schliermann, V. Trapp, W. Schuetz, K. Bohmhammel, G. Wolf, J. Garche, J. Pow. Sourc. 84 (1999) 221.
[2] F.E. Pinkerton, B.G. Wicke, C.H. Olk, G.G. Tibbets, G.P. Meisner, M.S. Meyer, J.F. Herbst, J. Phys. Chem. B 104 (2000) 9460.
[3] R.T. Yang, Carbon 38 (2000) 623.
[4] H.G. Schimmel, G.J. Kearley, M.G. Nijkamp, C.T. Visser, K.P. de Jong, F.M. Mulder, Chem. A Eur. J., 2003, in press.
[5] M.G. Nijkamp, Hydrogen Storage Using Physisorption. PhD thesis, Inorganic Chemistry and Catalysis, Debye Institute, Utrecht University, P.O. Box 80083, 3508 TB Utrecht, The Netherlands, April 2002.
[6] J.H. de Boer, The Dynamical Character of Adsorption, Clarendon Press, Oxford, 1968.
[7] M.L. Toebes, J.H. Bitter, A.J. van Dillen, K.P. de Jong, Catal. Today 76 (2002) 33.
[8] B.L. Mojet, M.S. Hoogenraad, A.J. van Dillen, J.W. Geus, D.C. Koningsberger, J. Chem. Soc., Far. Trans. 93 (1997) 4371.
[9] A. Chambers, C. Park, R.T.K. Baker, N.M. Rodriguez, J. Phys. Chem. B 102 (1998) 4253.
[10] C. Park, P.E. Anderson, A. Chambers, C.D. Tan, R. Hidalgo, N.M. Rodriguez, J. Phys. Chem. B 103 (1999) 10572.
[11] P. Chen, X. Wu, J. Lin, K.L. Tan, Science 285 (1999) 91.
[12] W.-F. Du, L. Wilson, J. Ripmeester, R. Dutrisac, B. Simard, S. Dénommée, Nano Lett. 2 (2002) 343.
[13] P.M. Ajayan, V. Ravikumar, J.C. Charlier, Phys. Rev. Lett. 81 (1998) 1437.
[14] M.G. Nijkamp, J.E.M.J. Raaymakers, A.J. van Dillen, K.P. d Jong, Appl. Phys. A 72 (2001) 619.
[15] G. Vidali, G. Ihm, H.-Y. Kim, M.W. Cole, Surf. Sci. Rep. 12 (1991) 135.
[16] A.C. Dillon, K.M. Jones, T.A. Bekkedahl, C.H. Klang, D.S. Bethune, M.J. Heben, Nature 386 (1997) 377.
[17] H.J. Sun, J. Phys Chem. 102 (1998) 7338.
[18] J. Stride F.M. Mulder, S.J. Picken, P.H.J. Kouwer, M.P. d Haas, L.D.A. Siebbeles, G.J. Kearley, J. Am. Chem. Soc. 125 (2003) 3860.
[19] Timofei Krouglov, Wicher H. Kraan, Jeroen Plomp, M. Theo Rekveldt, Wim G. Bouwman, J. Appl. Cryst. 36 (2003) 816–819.
[20] M.T. Rekveldt, W.G. Bouwman, W.H. Kraan, O. Uca, S. Grigoriev, S. Habicht, T. Keller, Neutron Spin Echo, in: Mezei, Pappas, Gutberlet (Eds.), Lecture Notes in Physics: Elastic Neutron Scattering Measurements Using Larmor Precession of Polarised Neutrons (Chapter), vol. 601, Springer, Berlin, 2003, pp. 87–99.
[21] M. Eswaramoorthy, R. Sen, C.N.R. Rao, Chem. Phys. Lett. 304 (1999) 207.